eprints@whiterose.ac.uk
https://eprints.whiterose.ac.uk/

Towards sensitivity analysis: 3D venous modelling in the lower limb

Magdalena Otta[1,2,3][0000−0002−8062−1354], Karol Zając[1][0000−0003−1393−8236], Maciej Malawski[1,6][0000−0001−6005−0243], Ian Halliday[2,3], Chung Lim[5], Janice Tsui[4,5], and Andrew Narracott[2,3][0000−0002−3068−6192]

[1] Sano Centre for Computational Medicine, Kraków , Poland (https://sano.science/)
m.otta@sanoscience.org
[2] Division of Clinical Medicine and Population Health, University of Sheffield, Sheffield, UK
motta1@sheffield.ac.uk
[3] Insigneo Institute for *in silico* medicine, University of Sheffield, Sheffield, UK
[4] University College London, London, UK
[5] Royal Free London NHS Foundation Trust, London, UK
[6] Faculty of Computer Science, AGH University of Kraków, Kraków, Poland

Abstract. Deep vein thrombosis (DVT) of the lower extremity frequently leads to long-term complications known as post-thrombotic syndrome (PTS). The current clinical workflow for DVT and PTS treatment lacks sufficient evidence. The significance of the variation in the venous anatomy is yet to be understood. We report an analysis of a set of idealised 3D geometries of iliac vein unification to assess the importance of shape variability, inflow conditions, and viscosity on local haemodynamics - specifically on the wall shear stress metrics. Regions of low wall shear stress and high oscillating shear index have been associated with prothrombotic effects on the walls of blood vessels. A detailed steady state analysis focused on the wall shear stress distributions below three thresholds ($< 0.15Pa, < 0.10Pa < 0.05[Pa]$). The preliminary work in the transient state focused on the oscillating shear index above three thresholds ($> 0.25, > 0.35, > 0.45$). We found that all the variations implemented had an effect on the size and shape of the absolute vein wall area subject to the shear metrics of choice under the assumed flow conditions. The results obtained in this research will serve as a basis for the interpretation of patient-specific geometries of the iliac vein unification affected by deep vein thrombosis.

Keywords: deep vein thrombosis · post-thrombotic syndrome · venous modelling · CFD · sensitivity analysis

1   Introduction

Post-thrombotic syndrome (PTS) is the most common long-term complication of deep vein thrombosis (DVT) of the lower extremity, a disease caused by abnormal blood clotting, often found in the iliofemoral region of the body [1]. Up to 100 in 100,000 experience the first episode of symptomatic DVT every year. Up to 50% will develop PTS in two years and about 33% will experience recurrent DVT within ten years [2]. Iliofemoral DVT usually presents the most severe symptoms and is more likely to cause PTS than other anatomical variants of the disease. The way DVT and PTS manifest can vary significantly between patients, making treatment challenging. In addition, current clinical workflows often lack strong evidence to support their effectiveness. More research is needed to understand the impact of variations in venous anatomy on the haemodynamics of the affected area. Blood flow changes, particularly stasis (prolonged blood residence) and recirculation, have been identified as a risk factor for thrombus development, but due to the potential variability of these changes in complex venous anatomy, this is not currently well understood.

Computational Fluid Dynamics (CFD) is an established approach for modelling blood flow in segments of the cardiovascular system. A short review of key concepts of cardiovascular modelling is provided by [3]. CFD analysis is typically based on solving the Navier-Stokes equations. Numerical solutions are obtained from the finite volume/element discretisation method. Depending on the purpose of the study, a numerical model can range from 0D to 3D in dimensionality. Representing and simulating all vessels in a numerical model would be impractical due to the high computational cost. Typically, vessels are lumped into several components that represent specific anatomical regions in reduced-order models (0D, 1D), sufficiently detailed to resolve the physiology of the real system [4], or localised segments of the cardiovascular system are modelled in detail (3D). Because DVT is a localised problem, 3D modelling could help to understand the local haemodynamics in the region of the thrombus. For any 3D model, the nature of the fluid dynamics depends on both the local 3D model geometry and the boundary conditions applied to this local 3D domain. Interpretation of the impact of flow changes on the biological response can be supported using parameters derived from the results of a CFD analysis. The local wall shear distribution has been associated with the behaviour of endothelial cells. The low wall shear stress region may cause endothelial dysfunction leading to an increased risk of thrombosis initiation and progression. Although the subject has been investigated in the context of arterial networks [5], the literature on wall shear stress that promotes thrombosis in the venous system remains scarce with a few exceptions, including ref. [6] that used CFD to quantify haemodynamics in the portal venous system looking at the area of the wall regions exposed to low wall shear stress before and after splenectomy. A more relevant example, ref. [7] investigated the impact of iliac vein stenting on blood flow, by simulating haemodynamics, including wall shear stress (WSS) and oscillatory shear index (OSI), in patient-specific geometries after stenting to assess the risk of resteno-

sis. These studies focused on patient-specific geometries without investigating the relative influence of controlled variation on the calculated metrics.

This work focuses on the possibility of applying and personalising blood flow models to aid clinical decisions in the treatment of deep vein thrombosis. We investigated the significance of changes in vessel geometry, boundary conditions, and viscosity in predicted wall shear stress metrics in a set of idealised geometries of iliac vein unification.

2   Methods

In previous work, we developed a 0D model of the circulation in the lower extremities [8], including arterial inflow, capillaries, and venous outflow to investigate the influence of anatomical variability on global haemodynamics in the lower extremity; we achieved this by varying the radii of the vessels ($\pm10\%$) from their reference values taken from the literature [9]. Through this analysis, we characterised the influence of such variability on the inflow and outflow in the iliofemoral region, particularly the unification of the internal and external iliac veins into a common iliac vein. In this study, these flow conditions were used to define boundary conditions for simulations using computational fluid dynamics (CFD) for a set of idealised 3D geometries of the iliac veins to investigate interactions between variability of these boundary conditions and other factors associated with the local definition of the 3D model on the nature of the detail of the flow in this region. Steady-state simulations were conducted in ANSYS Fluent. Preliminary sensitivity analysis of the 3D flow field was performed by varying the geometry, boundary conditions, and blood viscosity to investigate their relative influence on the distribution of WSS, a parameter related to blood coagulation and the development of thrombuses [10].

2.1   The base state simulation

All variations were considered relative to a single case, termed the *base case* or the *base state*. To reflect a realistic anatomical configuration, the geometry had two inlets and one outlet (Fig. 1). The parameters of each considered vessel were taken from Ref. [9] as provided in Table 1. The simulation was set as steady state *laminar* flow with constant density ρ (*incompressible*) and constant viscosity μ (*Newtonian*), with $\rho = 1050 kg \cdot m^{-3}$ and $\mu = 0.0035 Pa \cdot s$. To ensure developed flow profiles, velocity inlets were prescribed with parabolic profiles. The outlet reference pressure was set to zero. For the internal iliac vein (small inlet), the maximum velocity of the parabolic profile was $U_{max|int} = 0.52 m/s$ and for the external iliac vein (large inlet) $U_{max|ext} = 0.16 m/s$. These values were defined to match the volume flow rate obtained from previous simulations using the 0D model. To avoid a significant influence of the zero pressure outlet condition on the flow field within the region of interest, close to the unification of the veins, the outlet vessel was extended from its physiological length to ten times its diameter, that is, from $58 mm$ to $115 mm$.

Table 1. Iliac veins - geometrical parameters

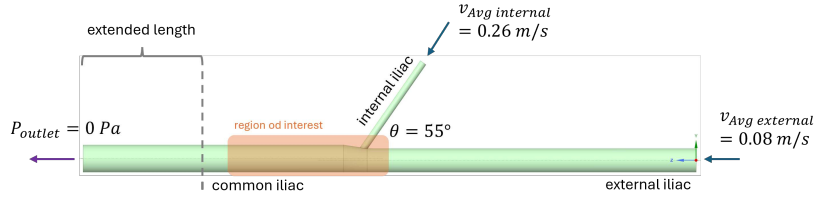| vein	d [mm]	L [mm]
external iliac	10.0	144.0
internal iliac	3.0	50.0
common iliac	11.5	58.0

Fig. 1. Base case setup: base geometry with straight vessels and 55-degree angle between internal and external iliac veins; common iliac vein (outlet) extended from real length to ten times its diameter; inlets of fixed average velocity from the 0D model and zero-pressure outlet. Region of interest - expected low shear stress region highlighted close to the join of the vessels.

2.2   Mesh sensitivity

Mesh sensitivity was performed for the base state geometry, analysing pressure and velocity metrics, to obtain a mesh with sufficient resolution at an acceptable computational cost. Meshes of five different resolutions were considered, four with global refinement of maximum element lengths of $1mm$, $0.5mm$, $0.25mm$ and $0.2mm$, and one with additional local refinement using a sphere of influence in the region around the unification with maximum element edge length of $0.25mm$ and refined edge length of $0.15mm$ (Fig. 2). The meshes were constructed from polyhedral elements. The finest refinement level was chosen considering the available computational resources. Each mesh had four inflation layers applied to the wall with a growth rate of 1.2. Fig. 2 provides an overview of the five levels of mesh refinement that display the grid at the boundaries and on the cut plane through the long axis of the unification. To assess the quality of the mesh, we considered the variation in velocity and pressure metrics, as well as the area of the wall subject to low values of wall shear stress with mesh refinement level.

2.3   Variation in vessel geometry

The variation of vein geometry was considered by creating three subsets of idealised iliac veins. The first subset included a variation in the angle between the internal and external iliac vein $\pm25°$ from the base state of $55°$ resulting in geometries with angles from $30°$ to $80°$. The second subset assumed a variation in the global curvature (simple, further referred to as type i) of the external to common iliac vein axis with the radius of curvature at $5mm$, $10mm$ and $15mm$. The

third subset assumed variation in the curvature of each vein separately (complex, further referred to as type ii) with the curvature radii between $5mm$ and $15mm$. In both subsets of curvature changes, the choice of the bending direction was dictated by that observed in medical images of real iliac vein unifications. Two types of vein connection were investigated for the base case and representative curvature variations: (1) the diameter was assumed constant along each vessel length and a tapered element was implemented to connect cross sections of different sizes, (2) the inlet and outlet diameters of the external and common iliac vein were set according to anatomical information from the literature, and a gradual transition in size was implemented along the vessel axes.

2.4   Variation in the inflow conditions

The variation in the inflow conditions to the internal and external iliac veins was considered by incrementally changing each inlet velocity over a range of $\pm 20\%$ from their average base values obtained from the 0D simulations, $0.26m/s$ and $0.08m/s$, respectively. This resulted in a range of $(0.208, 0.312)m/s$ for the internal iliac vein and $(0.064, 0.096)m/s$ for the external iliac vein. The parabolic velocity profiles for the base case and the variation extremes are shown in Fig. 4 A. In total, 25 steady-state simulations were performed to vary the inflow conditions for the geometry in the base state, 9 simulations changing inflow conditions for the simple (type i) change in curvature, and 9 for the complex (type ii) change in curvature.

2.5   Variation in blood viscosity

The viscosity of the blood was incrementally varied from the constant base value of $0.0035Pa \cdot s$ to $0.0055Pa \cdot s$ (the literature value for the maximum constant viscosity of the blood) for representative cases of each subset of variation of geometry. The use of a constant viscosity assumes that the blood behaves as a Newtonian fluid, which is true for large blood vessels (fluid as a continuum) and shear rates greater than $100s^{-1}$, which is generally true in the arteries. Shear rates in the venous circulation can be much lower than this, and models such as the Carreau model [11] allow the shear-thinning properties of blood to be included, representing non-Newtonian behaviour. To investigate the influence of non-Newtonian blood viscosity on the flow field, we repeated analyses using a Carreau model given by Eq. (1). The effective viscosity μ_{eff} is a variable of the shear rate $\dot{\gamma}$ and determined by infinite-shear viscosity μ_∞, zero-shear viscosity μ_0, time constant λ and the power-law index n.

$$\mu_{eff}(\dot{\gamma}) = \mu_\infty + (\mu_0 - \mu_\infty)(1 + (\lambda\dot{\gamma})^2))^{\frac{n-1}{2}} \tag{1}$$

At low shear rates, $\dot{\gamma} \ll 1/\lambda$, μ_{eff} approaches viscosity μ_0 and at high shear rates, viscosity μ_∞. At intermediate shear rates ($\dot{\gamma} \gtrsim 1/\lambda$), the model assumes a power-law fluid. For the purpose of this investigation, the infinite shear viscosity μ_∞ was set to $0.0035Pa \cdot s$, zero-shear viscosity μ_0 was set at $0.056Pa \cdot s$, the

power law index n was set at 0.35, and the time constant λ, at $3.3s$ based on representative values from the literature [12]. The plot of the resulting effective viscosity versus the shear rate is shown in Fig. 4B.
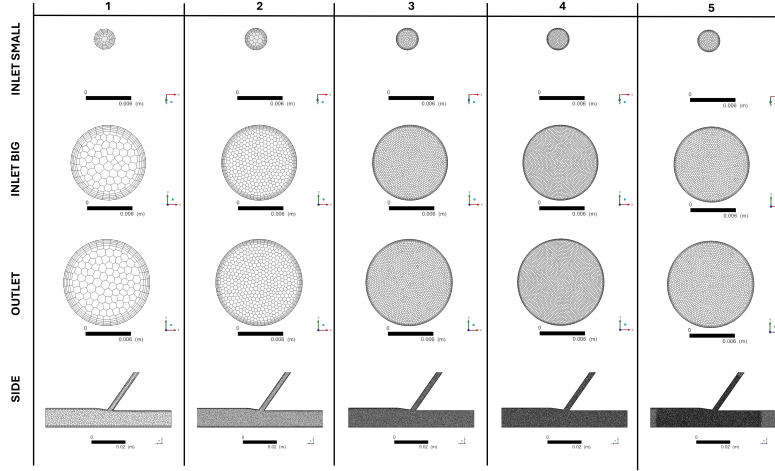

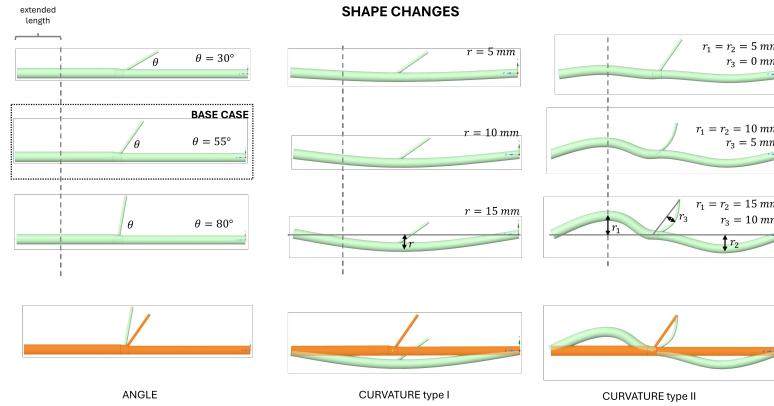**Fig. 2.** Five levels of refinement of the investigated meshes

Fig. 3. Top three rows: variation in geometry - three subsets: (1) unification angle change, (2) curvature change (type i), (3) curvature change (type ii), in each column the cases are referred to as (0,1,2) from top to bottom; **bottom row:** the geometry change wrt base case.
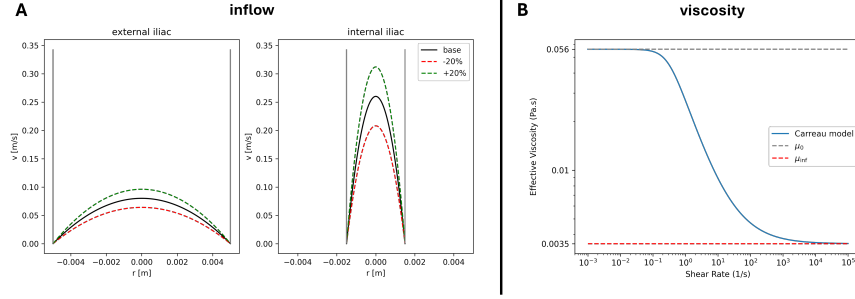
Fig. 4. (A) Parabolic profiles of inlet velocity for the base case and $\pm 20\%$ of maximum velocity for each vessel; (B) Carreau model for non-Newtonian viscosity.

2.6 Preliminary transient analysis

Preliminary work was performed to repeat all simulations (geometry, boundary conditions, and viscosity variation) in the transient state with oscillating inlet velocities defined by Eq. (2) assuming the parabolic inlets of the steady state $U_{profile|int}$ and $U_{profile|ext}$ for the internal and external iliac vein, respectively. The signal was assumed sinusoidal (justified by the results of Muller and Toro [9] in the considered region) with a frequency of $f = \frac{80}{60}$ equivalent to the heart rate of $80bpm$.

$$
\begin{aligned}
U_{int} &= U_{profile|int} \cdot (sin(2\pi f) + 1) \\
U_{ext} &= U_{profile|ext} \cdot (sin(2\pi f) + 1)
\end{aligned}
\tag{2}
$$

The oscillations in inlet velocities predicted by the 0D model were negligible, but the model did not assume any external sources of oscillation such as respiratory effects or the calf muscle pump. Therefore, the velocity values predicted by the 0D model were taken as average values of the oscillatory signal, and the amplitude of the oscillations was artificially increased. A total of 10 transient simulations were performed in this initial stage.

2.7 Metrics of interest

In steady state, the impact of the described changes in vein geometry, boundary conditions, and flow properties on local haemodynamics was evaluated by computing the surface area of the vessel wall exposed to low WSS. Changes in distribution size and shape were analysed using three threshold values: ≤ 0.15 Pa, ≤ 0.10 Pa, and ≤ 0.05 Pa. In the transient analysis, we have looked at the oscillating shear index (OSI) defined by Eq. (3) where we approximate the integrals over one period of the inlet signals, T.

$$
OSI = \frac{1}{2} \left(1 - \frac{\left| \int_0^T WSS \, dt \right|}{\int_0^T |WSS| \, dt} \right) \approx \frac{1}{2} \left(1 - \frac{|\overline{WSS}|}{\overline{|WSS|}} \right)
\tag{3}
$$

with $|\overline{WSS}|$ being the magnitude of the time-averaged WSS and $|WSS|$ - the time-averaged magnitude of WSS [13]. The OSI ranges between 0 and 0.5 where 0 indicates unidirectional flow and 0.5 fully reversible flow. The closer the OSI value to 0.5 the more oscillatory the WSS vector will be. The OSI distributions were analysed using three threshold values: $> 0.25, > 0.35, > 0.45$. All thresholds were set to values similar to those reported in other studies [6, 7]. Both metrics are assumed to be associated with pro-thrombotic effect on the endothelial cells of the vein wall.

2.8   Computing details

In total, we conducted 50 steady state simulations and 10 transient simulations. All were performed using ANSYS R2 2024 software, from the creation of idealised geometry in SpaceClaim 2024 to the meshing and simulation in Fluent R2 2024. The workflow was automated using the PyFluent library, enabling efficient script-based control of both meshing and solving processes. A batch processing approach was implemented to allow for parametrised execution through a CSV file. This setup enabled systematic variation of key parameters, including minimum and maximum mesh element sizes, maximum cell length, inlet velocities, blood viscosity, and solver-specific settings such as time-step size, number of time steps, and number of iterations. To run multiple simulations in parallel, batch jobs were submitted as an array job in the Slurm queueing system, with each instance running a specific combination of mesh configuration and solver settings. The implementation supported steady- and transient-simulations. Meshing was performed using 4CPUs, requiring approximately 10 minutes per case. The steady-state simulation on 4 CPUs took around an hour and required up to 50GB of RAM for highly refined global meshes. Transient simulations posed a greater challenge, each taking 4 hours on 192 CPUs with 90GB memory usage, and producing about 50GB of output data per case with 3 seconds of simulated flow.

3   Results

This section describes the results of the performed simulation addressing each section of the Methods.

3.1   The base state simulation

In steady state, the metric of interest is the wall area subject to a low WSS below three different thresholds. Fig. 5 shows an example of such a solution viewed in the XZ plane of the vessel geometry, where the area under each of the three thresholds considered is marked as a different-colour contour. The solution was obtained at mesh refinement level 4 (element length of $0.2mm$ as described in the Methods). The refinement was chosen on the basis of the mesh sensitivity investigation.
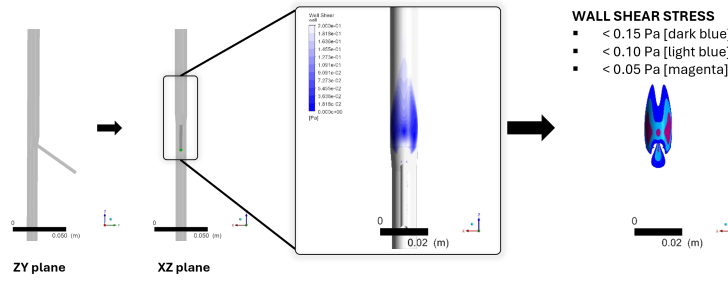
Fig. 5. Flow field obtained in the base state simulation.

3.2   Mesh sensitivity

To assess the necessary mesh refinement, the base case was simulated for the five mesh refinement levels described in Methods. The low wall shear stress distributions obtained from each simulation are shown in Fig. 6. Pressure and velocity metrics were also considered in this assessment, but tend to converge at smaller mesh refinements. In this context, the convergence means that there are little to no changes in the distribution with an increase in the mesh resolution. The results showed that refinement levels 1 and 2 were too coarse to capture the features of the WSS distribution that only appeared at refinement level 3. The distributions from refinement levels 4 and 5 still showed some small changes, but the dominant features had already been resolved. Considering the computational cost associated with running each mesh type, we decided to run all steady-state simulations at mesh refinement level 4 (element size $0.2mm$).
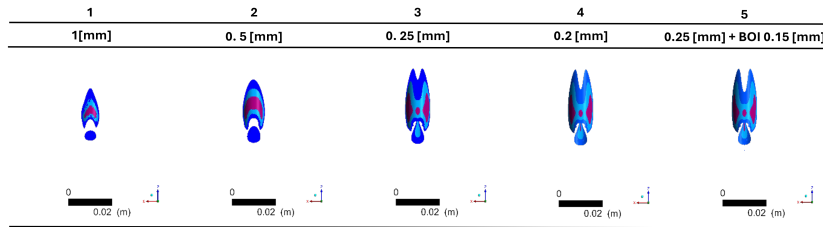

Fig. 6. The change in flow field with increasing mesh refinement.

3.3   Variation in vessel geometry

The variability in the geometry altered the absolute area and distribution of low WSS. The contours of the low WSS distributions obtained from simulations of different geometries are shown in Fig. 7A. The associated ranges for the change

in the absolute area of the low WSS below the three thresholds considered are summarised in Table 2. For the change in angle from 30 to 80 degress, the WSS area ($< 0.05, < 0.10, < 0.15$ [Pa]) varied from (196, 428, 687) to (16, 123, 269) mm^2. For the change in simple curvature (type i) from the radius of curvature $r = 5mm$ to $r = 15mm$, the area varied from (29, 267, 514) to (21, 209, 568) mm^2. For the change in the complex curvature (type ii) from the radius of curvature $r = 5mm$ to $r = 15mm$ the area ranged from (74, 243, 448) to (53, 315, 452) mm^2. It is worth pointing out that in type i curvature, when the radius of curvature was increased, the absolute wall area of WSS $< 0.05Pa$ and WSS $< 0.10Pa$ decreased, while for WSS $< 0.15Pa$ it increased. For type ii curvature, the area of WSS $< 0.05Pa$ decreased, and for the other two thresholds it increased with increasing radii of curvature.

The effect of varying the type of connection between veins (tapered element vs. gradual transition) on the calculated WSS and OSI distributions was small compared to those caused by changes in the curvature and angle of unification.

3.4   Variation in the inflow conditions

The variability in the inflow conditions altered the absolute area and distribution of the low WSS for each geometry considered. Fig. 7B shows a subset of low WSS areas obtained by varying the inflow velocities in the base geometry. The associated ranges for the absolute area of low WSS are summarised in Table 3. Both the area and the shape of the distribution change for each combination of the inlet conditions. Similar trends were observed for changes in the inflow velocity in the curved type i2 geometry and the curved type ii2 geometry.

3.5   Variation in blood viscosity

The variability in viscosity altered the absolute area and distribution of the low WSS for each case considered. The effect of varying constant viscosity on the range of the low WSS absolute area size for different vessel geometries is summarised in Table 4 and Fig. 8 shows the distributions for Newtonian viscosity at $0.0035Pa \cdot s$, $0.0045Pa \cdot s$ and $0.0055Pa \cdot s$ vs. the non-Newtonian Carreau viscosity model in the base geometry. Increasing the constant viscosity generally leads to a decrease in the low WSS area. Considering a non-Newtonian model of viscosity proved to have an effect on the shape and size of the low WSS distributions.
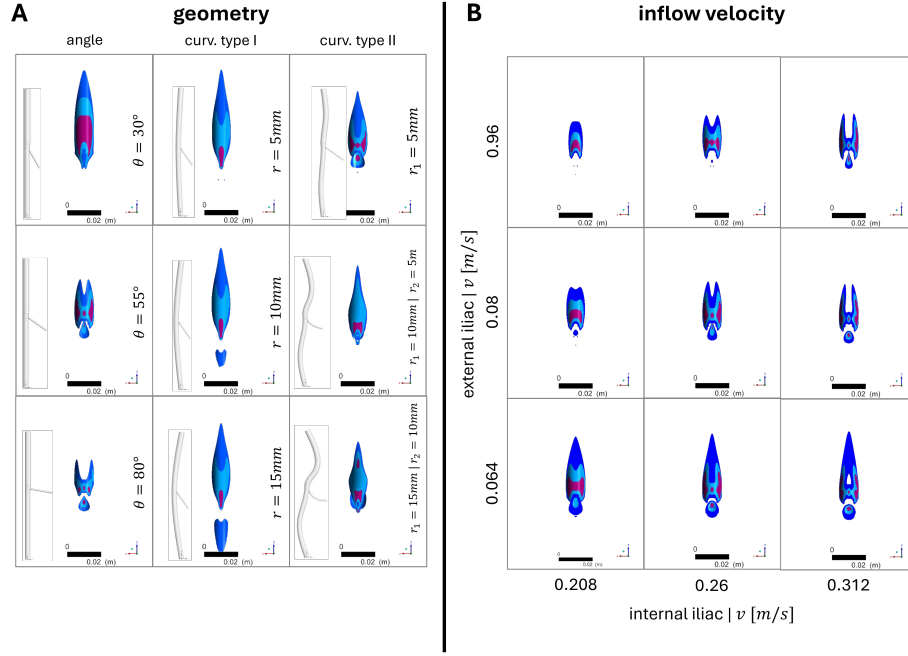
Fig. 7. Low WSS distributions for the three thresholds considered: (A) for different shapes of the iliac vein unification; (B) for different inflow velocities in the base geometry.

Table 2. Change in the vessel wall area subject to the low wall shear stress due to geometry change

GEOMETRY CHANGE - WSS area [mm^2]			
	Angle	C Type i	C Type ii
WSS < 0.05 [Pa]	$16 - 196$	$21 - 25$	$37 - 74$
WSS < 0.10 [Pa]	$123 - 428$	$209 - 266$	$243 - 315$
WSS < 0.15 [Pa]	269 - 687	514 - 568	448 - 509

Table 3. Change in the vessel wall area subject to the low wall shear stress due to variation in the inlet velocity

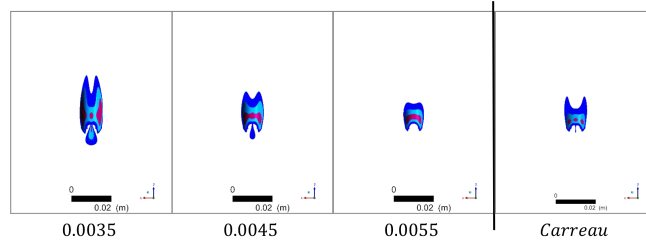| INLET VELOCITY CHANGE - WSS area [mm^2]			
	BASE	C Type i 2	C Type ii 2
WSS < 0.05 [Pa]	$28 - 114$	$9 - 293$	$38 - 129$
WSS < 0.10 [Pa]	$80 - 273$	$38 - 354$	$251 - 423$
WSS < 0.15 [Pa]	171 - 620	216 - 2163	356 - 1448

Fig. 8. Low WSS area identified for the base geometry for different values of constant viscosity and non-Newtonian Carreau model.

Table 4. Change in the vessel wall area subject to the low wall shear stress due to variation in viscosity

VISCOSITY CHANGE - WSS area [mm^2]			
	BASE	C Type i 2	C Type ii 2
WSS < 0.05 [Pa]	$3 - 84$	$3 - 21$	$18 - 53$
WSS < 0.10 [Pa]	$97 - 233$	$20 - 209$	$116 - 315$
WSS < 0.15 [Pa]	180 - 384	73 - 567	286 - 452

3.6 Preliminary transient analysis

The preliminary transient analysis identified regions of high OSI in approximately the same areas as regions of low WSS. Fig. 9 shows an example comparison between the identified low WSS region and the high OSI region for the same case. The distributions share some characteristics for each simulated case and respond similarly to the applied changes, but also display unique features. The choice of thresholds is not correlated between steady-state and transient cases, so one should be careful when drawing conclusions from the comparison.
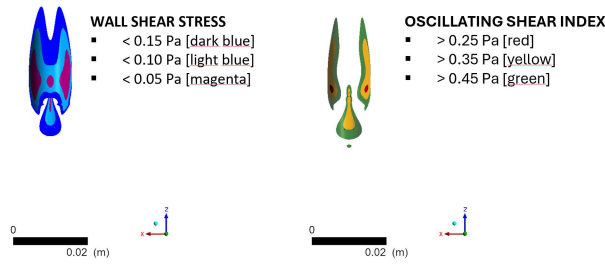

Fig. 9. Are subject to low WSS in the steady state (left) vs area subject to high OSI in transient state (right) for the base geometry. For the OSI: > 0.45 - green, > 0.35 - yellow, > 0.25 - red.

4 Discussion

In this study, we simulated a set of idealised geometries of iliac vein unification to assess the relative importance of shape variation, inflow conditions, and viscosity in the predicted metrics of wall shear stress. The choice of changes was informed by the available clinical data for the geometries but was limited to simple changes in the angle between the vessels and the change in their curvature radii. A more thorough shape investigation would be challenging to perform with such a simple parametrisation. To achieve a more principled variation, methods such as statistical shape modelling could be used on a larger set of idealised and patient-specific geometries of the considered veins. It is part of ongoing work as a means of generating samples of variable geometry for uncertainty investigation, but it is beyond the scope of this paper.

The change in average velocity by $\pm 20\%$ was considered sensible given the values predicted by the 0D model in earlier analyses. It may not cover the true variability in this region between patients, but it provides a way to investigate the effect of flow changes in the absence of experimental data. The range of variation in constant viscosity was informed by the values reported in the available literature. Given the nature of the venous flow, non-Newtonian effects may be of significance, and a simple non-Newtonian model (Carreau) was used to check if it affects the metrics of interest. Although changes were observed, the parameters of the model were based on the available literature due to the lack of experimental data in the region of interest. Each of the investigated variations had an effect on the predicted wall shear distributions, and it is difficult to rank the effects according to their significance.

Flow parameter variation (inflow, viscosity) could benefit from a more advanced approach, for example, using formal Sobol analysis to assess the uncertainty in the predicted metrics, but it is beyond the scope of this paper. It would require a more in-depth investigation of the parameter space, including filtering out unphysical parameter combinations. In addition, formal variance-based sensitivity analyses require a large number of input samples to obtain statistically significant outcomes. Depending on the number of input parameters, this could easily scale to thousands of simulations and would pose a greater computational challenge - if at all feasible - especially in the transient case. The approach presented in this work is more similar to local sensitivity analysis, and conducting it on very idealised models allows us to quantify the relative influence of variation in individual aspects of the flow problem that would be impossible to distil from patient-specific geometries, which will be analysed in the future work.

A mesh sensitivity study was performed to choose a grid that would resolve the critical features of predicted haemodynamics at an acceptable computational cost. Based on the steady-state simulation of the base geometry, we chose a refinement level with an element size of $0.2mm$. The global refinement to an element size of $0.15mm$ was computationally intractable with the available resources. Applying this refinement locally close to the unification substantially increased the computational cost without causing a significant change in the pre-

dicted haemodynamics. More computationally intensive transient analysis posed a greater challenge for the same mesh element size, consuming significantly more high-performance computing resources.

We assumed that wall shear stress metrics could serve as thrombosis risk metrics: low WSS in the steady state and high OSI in the transient state. This is an assumption based on the available literature. The choice of thresholds is subject to a biological and clinical interpretation of the specific location in the vasculature, but it does not undermine the findings of this research. An adjustment of the threshold to ones based on experimental data would be straightforward.

Vein compliance and fluid-structure interactions (FSI) were effectively ignored, which could be of significance in veins that are highly compliant compared to arteries. This assumption affects the flow dynamics and pressure distribution, which in turn may lead to inaccurate estimations of the wall shear stress. The choice was made for two reasons: (1) the complexity of the assumptions was incrementally increased to ensure that the importance of each step is assessed, (2) there are no clinical data collected on venous compliance of the iliac veins during standard clinical practice, and applying a generalised condition to all patients could result in more inaccurate predictions than with the rigid body assumption. It would only work if the vessel's environment was well known and other aspects such as respiratory effects were investigated.

The results obtained from the simulated cases will be used for the interpretation of patient-specific clinical data. Knowing the relative effect of the changes investigated on the shear metrics could help predict the expected effects of DVT treatment.

5   Conclusion

This work investigated the influence of geometry, inflow conditions, and viscosity on wall shear stress metrics – assumed to be related to prothrombotic responses – in 3D simulations of idealised iliac vein unifications with a detailed steady-state analysis and preliminary transient analysis. The results revealed substantial differences in the predicted metrics between each simulated case. Although further work is required to complete the analysis of the transient state, the investigations conducted provide a basis for interpretation of patient-specific vein geometries.

Disclosure of Interests. The authors declare that there is no potential conflict of interest.

References

1. Baldwin, M.J. et al.: Post-thrombotic syndrome: a clinical review. Journal of Thrombosis and Haemostasis, **2**(11), 795-805 (2013), (https://doi.org/10.1111/jth.12180)
2. Kakkos, S.K. et al.: Guidelines on the Management of Venous Thrombosis. Eur J Vasc Endovasc Surg., **2**(61), 9-82 (2021), (https://doi.org/10.1016/j.ejvs.2020.09.023)
3. Morris, P.D. et al.: Computational fluid dynamics modelling in cardiovascular medicine. Heart, **2**(102), 18-28 (2016), (https://doi.org/10.1136/heartjnl-2015-308044)
4. Figueroa, C.A. et al.: Encyclopedia of Computational Mechanics. 2nd edn. John Wiley & Sons Ltd. (2017)
5. Belkacemi, D. et al.: Intraluminal Thrombus Characteristics in AAA Patients: Non-Invasive Diagnosis Using CFD. Bioengineering **10**, 540 (2023), https://doi.org/(10.3390/bioengineering10050540)
6. Wang, T. et al.: Predicting the risk of postsplenectomy thrombosis in patients with portal hypertension using computational hemodynamics models: A proof-of-concept study, Clinical Biomechanics, **98**, 105717 (2022) (https://doi.org/10.1016/j.clinbiomech.2022.105717)
7. Fan, Z. et al.: Insights from Computational Fluid Dynamics and In Vitro Studies for Stent Protrusion in Iliac Vein: How Far Shall We Go?. Cardiovasc Eng Tech, **16**, 79–90 (2025), (https://doi.org/10.1007/s13239-024-00758-7)
8. Otta, M., et al.: Sensitivity Analysis of a Model of Lower Limb Haemodynamics. In: Groen, D., de Mulatier, C., Paszynski, M., Krzhizhanovskaya, V.V., Dongarra, J.J., Sloot, P.M.A. (eds) Computational Science – ICCS 2022. Lecture Notes in Computer Science, vol 13352. Springer, Cham. (2022), (https://doi.org/10.1007/978-3-031-08757-8_7)
9. Müller, L.O. and Toro, E.F.: A global multiscale mathematical model for the human circulation with emphasis on the venous system, International Journal for Numerical Methods in Biomedical Engineering, **30**, 681-725 (2014), (https://doi.org/10.1002/cnm.2622)
10. Mukul S.G. and Scott L.D.: Adhesion of normal erythrocytes at depressed venous shear rates to activated neutrophils, activated platelets, and fibrin polymerized from plasma. Blood **100**(10): 3797–3803 (2002), (https://doi.org/10.1182/blood-2002-03-0712)
11. Kannojiya, V. et al.: Simulation of Blood as Fluid: A Review From Rheological Aspects, in IEEE Reviews in Biomedical Engineering, **14**, 327-341 (2021), (https://doi.org/10.1109/RBME.2020.3011182)
12. Junaidi, A.R. et al.: Simulation of non-Newtonian flow of blood in a modified laparoscopic forceps used in minimally invasive surgery. Computer Methods in Biomechanics and Biomedical Engineering, **24**(16), 1794–1806 (2021), (https://doi.org/10.1080/10255842.2021.1919884)
13. Soulis, J.V. et al.: Relative residence time and oscillatory shear index of non-Newtonian flow models in aorta, 2011 10th International Workshop on Biomedical Engineering, (https://doi.org/10.1109/IWBE.2011.6079011)